Earth and Planetary Science Letters 568 (2021) 117015

Contents lists available at ScienceDirect

Earth and Planetary Science Letters

www.elsevier.com/locate/epsl

Quantifying pyrite oxidation on continental shelves during the onset of Antarctic glaciation in the Eocene-Oligocene transition

Weiqi Yao [a,*], Stefan Markovic [b], Adina Paytan [c], Andrea M. Erhardt [d], Ulrich G. Wortmann [a]

[a] Department of Earth Sciences, University of Toronto, Toronto, Ontario, M5S 3B1, Canada
[b] Department of Physical and Environmental Sciences, University of Toronto Scarborough, Toronto, Ontario, M1C 1A4, Canada
[c] Institute of Marine Science, University of California–Santa Cruz, Santa Cruz, CA, 95064, USA
[d] Department of Earth and Environmental Sciences, University of Kentucky, Lexington, KY, 40508, USA

ARTICLE INFO

Article history:
Received 23 October 2020
Received in revised form 11 May 2021
Accepted 20 May 2021
Available online xxxx
Editor: L. Derry

Keywords:
sulfate
sulfur isotopes
oxygen isotopes
pyrite oxidation
Eocene-Oligocene transition

ABSTRACT

The Eocene-Oligocene transition (EOT) is characterized by a global cooling trend, falling sea levels, and the onset of Antarctic glaciation. Previous studies investigate the interactions and feedbacks between ocean circulation, weathering, and atmospheric CO_2 levels during this time. Here we explore the role of biogeochemical sulfur cycling, and report seawater sulfate isotope data across the EOT. Our data show that seawater sulfate $\delta^{34}S$ and $\delta^{18}O_{SO_4}$ values decline by 0.6‰ and 1.5‰, respectively, between 34.5 and 33 Ma. Quantitative modeling suggests that approximately 8,000 Gt of the sulfide previously stored in shelf sediments has been reoxidized and transferred to the marine sulfate pool. This reoxidation process proceeds through reactions similar to those associated with acid mine drainage, generating 24,500 Gt sulfuric acid. These numbers are of similar magnitude as those estimated for Pleistocene glaciations and must have affected marine pH and/or alkalinity.

1. Introduction

During the Eocene-Oligocene transition (EOT, sensu stricto ~33.9-33.5 Ma), the Earth system experienced a climatic transition from an ice-free greenhouse world to an icehouse with extensive polar glaciation, commencing with the onset of Antarctic glaciation (Kennett and Shackleton, 1976; Zachos et al., 2001; Coxall and Pearson, 2007; Liu et al., 2009). While evidence for small-ephemeral Antarctic ice sheets appeared already in the late Eocene (~38 Ma), sustained Antarctic glaciation did not occur before the earliest Oligocene (~34 Ma). The latter is marked by a +1‰ oxygen-isotope shift in benthic foraminifera records (i.e., Oi-1 event), consistent with glacial growth and associated changes in sea level (Miller et al., 1987; Zachos et al., 2001; Ivany et al., 2006; Coxall and Pearson, 2007; Katz et al., 2008; Kominz et al., 2008).

It has been hypothesized that this cooling trend is caused by lower atmospheric pCO_2 due to intensified physical and chemical weathering in the wake of the Tibetan Plateau uplift, increased thermal isolation of Antarctica and the development of the Antarctic Circumpolar Current, and/or possibly increased sulfate aerosol concentration (e.g., Zachos et al., 2001; DeConto and Pollard, 2003; Wortmann and Paytan, 2012; Basak and Martin, 2013). Irrespective of the cause for this cooling trend, associated changes to the hydrological cycle included glaciation and concomitant sea-level drop of 50 to 100 meters (Kominz et al., 2008; Miller et al., 2020). The sea-level drop may have exposed large areas (approximately 1.5×10^7 km^2) of the previously submerged continental shelves to oxidative weathering environments. Carbonate-buffered oxidation of sulfide minerals in continental margin sediments can produce sulfuric acid and subsequently dissolve carbonate minerals (e.g., $4FeS_2 + 15O_2 + 22H_2O + 8CaCO_3 \rightarrow 4Fe(OH)_3 + 8CaSO_4 \cdot 2H_2O + 8CO_2$; Berner, 1982; Garrel and Lerman, 1984). Several authors (e.g., Torres et al., 2014; Markovic et al., 2015) suggested that this CO_2 release might constitute climate stabilizing feedback over geologic timescales. Torres et al. (2017) hypothesized that the changes in the balance of silicate to sulfide weathering might have been an important negative feedback mechanism during the Last Glacial Maximum (LGM), and Kölling et al. (2019) proposed that sulfide oxidation might have triggered glacial terminations. Here we investigate the relation between sea-level controlled shelf area changes and sulfide oxidation and its potential climate impact during the onset of Antarctic glaciation in the Eocene-Oligocene transition.

2. Background

In anoxic marine sediments sulfate serves as the most abundant terminal electron acceptor for organic matter remineralization, and the principal reaction scheme of microbial sulfate reduction (MSR)

* Corresponding author.
E-mail address: weiqi.yao@mail.utoronto.ca (W. Yao).

https://doi.org/10.1016/j.epsl.2021.117015
0012-821X/

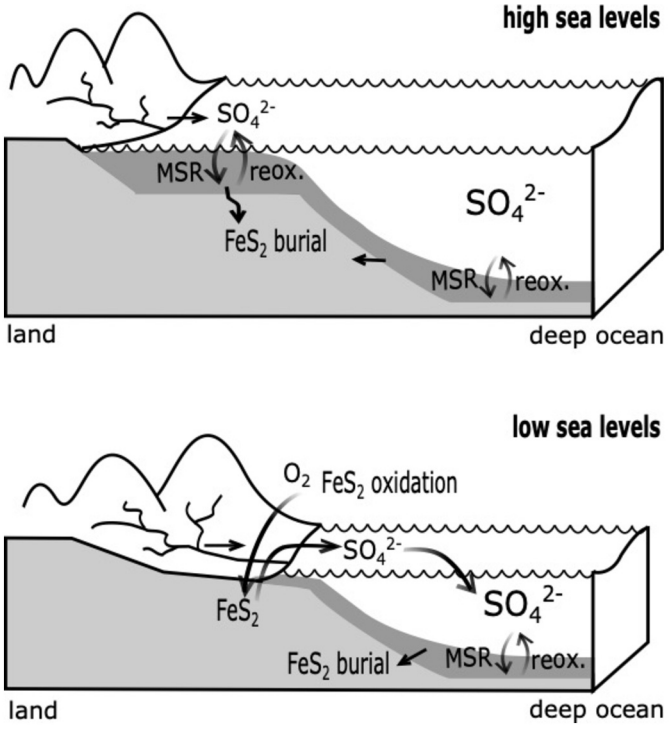

Fig. 1. Influence of sea-level variations on the oxidation of sedimentary pyrite on continental shelves and sulfate recycling within the ocean. Sulfate recycling and the subsequent pyrite burial are favorable on continental shelves during sea-level high stands; when sea level drops, sedimentary pyrite in newly exposed shelf sediments is oxidized to sulfate and enters the ocean via surface runoff. Sulfur cycling on continental slopes and abyssal plains is less likely affected by sea-level changes.

can be written as $2CH_2O + SO_4^{2-} \rightarrow 2HCO_3^- + H_2S$ (Berner, 1982; Jørgensen, 1982). A fraction of the sulfide produced binds with reactive iron to precipitate as pyrite (FeS_2), while the majority of the sulfide is subsequently reoxidized in a complex set of microbially mediated and abiotic redox reactions near the sediment-water interface and is ultimately returned as sulfate to the ocean (Jørgensen, 1982). Sulfate recycling through MSR and sulfide reoxidation constitutes the dominant sulfate flux in the modern ocean, with an estimated global rate between 8×10^{12} and 1×10^{14} mol/yr (Turchyn and Schrag, 2006; Bowles et al., 2014). The pyrite burial flux is about one to two orders of magnitude lower than the MSR flux (Jørgensen, 1982; Turchyn and Schrag, 2006; Markovic et al., 2016) and comprises approximately 40% of the total sulfur sink in the ocean (Burke et al., 2018).

Organic-rich anoxic sediments are common along continental shelves, and sea-level variations exert a prominent influence on subaerial erosion and accumulation of such sediments (Hay and Southam, 1977). Therefore, fluxes of MSR, sulfide reoxidation, burial and oxidative weathering of pyrite are sensitive to the extent of shelf area (Turchyn and Schrag, 2006; Markovic et al., 2015, 2016). During sea-level high stands, the shelf area expands, and MSR and pyrite burial are more prevalent; during sea-level low stands, the shelf area shrinks, MSR decreases, and the previously buried pyrite is reoxidized (Fig. 1).

Sulfate-reducing microorganisms preferentially break the ^{32}S-O bond, leaving the residual sulfate pool enriched in ^{34}S (Kaplan and Rittenberg, 1964; Chambers and Trudinger, 1979). Sedimentary pyrite is usually depleted in ^{34}S, which allows us to track global pyrite burial/oxidation fluxes. While the expression of S-isotope ($\delta^{34}S$) fractionation between sulfate and sulfide (up to 72‰) depends on a variety of factors, the two main drivers are cell-specific sulfate reduction rate and the availability of the carbon substrate (e.g., Sim et al., 2011; Leavitt et al., 2013). It is likely that changes in shelf size affect sedimentation rate and/or organic matter supply, which in turn affect the S-isotope fractionation between seawater sulfate and pyrite, with lower fractionation occurring in high sedimentation organic-rich shelve settings (Goldhaber and Kaplan, 1975; Leavitt et al., 2013; Rennie et al., 2018). Hence, in the following, we assume a negative correlation between global average S-isotope fractionation and shelf area (see details in Method and SI). Furthermore, shelf size also controls the net pyrite burial rate (Markovic et al., 2015). In this context, increased pyrite burial on expanded continental shelves during sea-level high stands results in a more positive seawater sulfate $\delta^{34}S$ value, while oxidation of substantial amounts of pyrite in response to sea-level falls decreases seawater sulfate $\delta^{34}S$.

On the other hand, oxygen isotope fractionation in sulfate occurs during MSR, sulfur disproportionation, and sulfide reoxidation. MSR proceeds through a chain of reversible enzymatic reactions (Mizutani and Rafter, 1973; Brunner et al., 2005), where kinetic fractionation and isotope exchange reactions with ambient water can drive the residual sulfate O-isotope ($\delta^{18}O_{SO_4}$) towards equilibrium values 25-29‰ higher than ambient water ($\delta^{18}O_{H_2O}$) at typical porewater temperatures and pH (Fritz et al., 1989; Böttcher et al., 1998; Wortmann et al., 2007; Zeebe, 2010; Wankel et al., 2014). The $\delta^{18}O_{SO_4}$ value of sulfate produced by microbial sulfur disproportionation is 8-21‰ higher than ambient water $\delta^{18}O_{H_2O}$, depending on the presence of scavengers reactive Fe(III) and/or Mn(IV) (oxyhydr)oxides (e.g., Böttcher and Thamdrup, 2001; Böttcher et al., 2005), while the sulfate produced by microbially mediated sulfide reoxidation is 0-8‰ more enriched in ^{18}O compared to ambient water (Van Stempvoort and Krouse, 1994; Balci et al., 2012). Due to the concurrence of different processes in natural environments, it is hard to differentiate contributions from these microbial processes based on O-isotope signatures. In contrast, abiotic sulfide oxidation incorporates oxygen from the ambient water into the sulfate product, resulting in sulfate with a $\delta^{18}O_{SO_4}$ value close to ~0‰; (Van Stempvoort and Krouse, 1994). During these processes, sulfur is constantly reduced and reoxidized, and only the net reduction of sulfate to sulfide affects seawater sulfate $\delta^{34}S$.

Typically, abiotic sulfide oxidation has a much slower reaction rate and is more favorable in abyssal environments where sediments are oxic and organic carbon limited, whereas microbially mediated sulfate recycling (i.e., MSR, microbial sulfide oxidation, and microbial disproportionation of elemental sulfur) predominantly takes place in organic-rich oxygen-limited sediments common on continental shelves (Van Stempvoort and Krouse, 1994; Turchyn and Schrag, 2006; Markovic et al., 2016). Therefore, when sea level rises, microbially mediated sulfate recycling will intensify globally, resulting in a more positive seawater sulfate $\delta^{18}O_{SO_4}$ value. When sea level falls, abiotic sulfate recycling will become more favorable, resulting in a more negative seawater sulfate $\delta^{18}O_{SO_4}$ value.

In the modern ocean, seawater sulfate S and O isotopes have a residence time on the order of 10 million years and 1 million years, respectively, exceeding the global oceanic mixing time by orders of magnitude (Claypool et al., 1980). Hence, it is widely considered that sulfate concentrations and isotope ratios are homogeneous throughout the global open ocean, reflecting the balance between its input and output fluxes to/from the ocean. We note that due to the slow rate of O-isotope exchange between sulfate and ambient water, seawater sulfate is out of isotopic equilibrium with seawater water within its residence time (Lloyd, 1968; Van Stempvoort and Krouse, 1994). Isotope compositions of seawater sulfate are faithfully and continuously recorded in pelagic barite due to direct precipitation from seawater and the refractory nature of barite. As such, we use pelagic barite as a proxy for reconstruct-

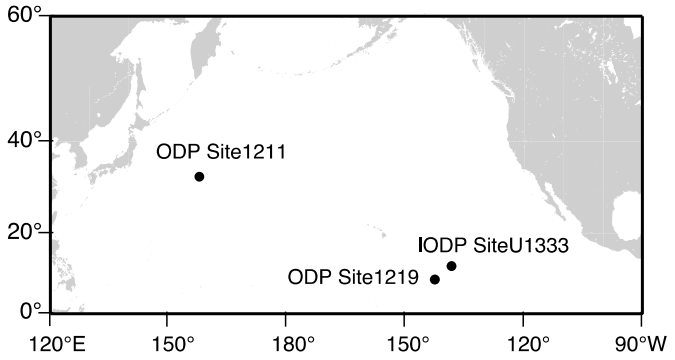

Fig. 2. Map of sample sites used in this study. The locations of ODP Site 1211 Hole A (32°0.1300′N, 157°50.9999′E, water depth 2907.5 m), ODP Site 1219 Hole A (7°48.0097′N, 142°0.9390′W, water depth 5063.3 m), and IODP Site U1333 Hole C (10°30.996′N, 138°25.146′W, water depth 4853.8 m) are after Bralower et al. (2002), Lyle et al. (2002), and Pälike et al. (2010), respectively.

ing seawater sulfate $\delta^{34}S$ and $\delta^{18}O_{SO_4}$ from the late Eocene to the early Oligocene.

3. Methods

We use pelagic barite separated from sediment samples from Ocean Drilling Program (ODP) Leg 198 Site 1211 Hole A at the Shatsky Rise in the Central Basin of the North Pacific Ocean, and ODP Leg 199 Site 1219 Hole A and Integrated Ocean Drilling Program (IODP) Expedition 320 Site U1333 Hole C in the Equatorial Pacific (Fig. 2). Sediments in sections sampled for this study consist of clayey radiolarian ooze and nannofossil ooze, with negligible pyrite and organic carbon contents. Sulfate concentrations in pore water are high (26-28.5 mM) throughout these cores (Bralower et al., 2002; Lyle et al., 2002; Pälike et al., 2010) and comparable to the modern seawater sulfate concentration of ~29 mM (Horita et al., 2002), implying negligible net sulfate reduction.

We select sediment samples spanning the E/O transition at an average temporal resolution better than 120 thousand years. The sediments are treated using a sequential leaching method to extract insoluble minerals (Paytan et al., 1993). The barite within this insoluble residue is examined with a scanning electron microscope (SEM) to verify that the pelagic barite has not been affected by diagenesis based on the morphology and size of barite crystals (see SI). We then use 1 mL supersaturated sodium carbonate solution to dissolve the barite in order to separate it from other insoluble O-bearing minerals in the residue (primarily some rutile; Makovic et al., 2016). We acidify the supernatant, reprecipitate barite by adding 2-5 mL 10% barium chloride, and dry the precipitates at 700 °C to get rid of hydration water in barite crystalline lattice before grinding them into powder for isotope analyses.

3.1. Isotope analyses

We measure sulfur and oxygen isotope ratios using an isotope ratio mass spectrometer system in continuous flow mode (CF-IRMS, Finnigan MAT 253) at the Geobiology Isotope Laboratory at the Department of Earth Sciences (University of Toronto). For S-isotope analysis, we weigh approximately 200 (±5%) µg barite powder with ~600 µg vanadium pentoxide powder (V_2O_5) as a catalyst into a tin capsule. Tin capsules are introduced into a Eurovector Elemental Analyzer (EA3000 series) and flash combusted in an oxygen atmosphere, generating sulfur dioxide (SO_2) as the analyte gas. S-isotope values are calibrated using three international barium sulfate standards with respect to Vienna Canyon Diablo Troilite (VCDT; Brand et al., 2014): NBS 127 (21.1‰), IAEA-SO-5 (0.5‰), and IAEA-SO-6 (−34.1‰). We use NBS 127 or in-house $BaSO_4$ standard (8.9‰) to track instrument drift, repeated measurements of which yield a 1σ error of ±0.1‰ or ±0.3‰, respectively.

For O-isotope analysis, we weigh approximately 200 (±5%) µg dried barite powder in a silver capsule. Silver capsules are introduced to an autosampler of the Hekatech high-temperature pyrolysis furnace and pyrolyzed with excess glassy carbon under a helium atmosphere, generating carbon monoxide (CO) gas as the analyte gas. O-isotope values are calibrated using four international standards with respect to Vienna Standard Mean Ocean Water (VSMOW; Brand et al., 2014): USGS32 (25.4‰), IAEA-SO-5 (12.1‰), NBS 127 (8.6‰), and IAEA-SO-6 (−11.4‰). We use NBS 127 to track instrument drift, repeated measurements of which yield a 1σ error of ±0.2‰.

3.2. Statistical analysis

We assign the age of each barite sample in accordance with the GTS2012 timescale (Gradstein et al., 2012) using the Neptune database, which converts biostratigraphic zones into absolute ages. Since the isotope value of seawater sulfate at any given time (t) depends to a certain degree on the value at a given time before ($t-\Delta t$), we estimate the "true" $\delta^{34}S$ and $\delta^{18}O_{SO_4}$ signals of seawater sulfate using a "local regression smoothing" module (LOESS; Cleveland, 1979) provided by the statistical software package R for the corresponding data set. The optimal "span" value is determined by the 10-fold cross validation (CV) technique through calculating the lowest average CV mean square error for the data set. The 95% confidence interval is calculated for each data point from the standard errors returned by the LOESS function.

3.3. The sulfur cycle model

We use mass conservation equations to model the sulfur cycle. The mass of seawater sulfate at any given time step is described as:

$$\frac{d}{dt}M_{SO_4} = F_V + F_{WE} + F_{WP} - F_{BE} - F_{BP}, \quad (1)$$

where M_{SO_4} denotes the mass of seawater sulfate, calculated from the ocean volume and the seawater sulfate concentration; F_V, F_{WE}, and F_{BE} denote the volcanic degassing flux, evaporite ($CaSO_4$) weathering flux, and evaporite burial flux, which are assumed to be constant throughout the model run, since there is no substantial evaporite precipitation/dissolution event or major volcanism event during the late Eocene – early Oligocene (e.g., Hansen and Wallman, 2003; Hay et al., 2006); F_{WP} and F_{BP} denote the total pyrite weathering flux and pyrite burial flux, respectively.

We calculate pyrite burial flux as the difference between MSR flux and sulfide reoxidation flux in/out of sediments:

$$F_{BP} = F_{MSR} - F_{REOX}, \quad (2)$$

where F_{MSR} denotes the MSR flux into sediments; F_{REOX} denotes the reoxidation flux (including abiotic and microbial sulfide reoxidation and sulfur disproportionation) out of sediments.

Combining Eq. (1) and Eq. (2), we obtain

$$\frac{d}{dt}M_{SO_4} = F_V + F_{WE} + F_{WP} - F_{BE} - F_{MSR} + F_{REOX} \quad (3)$$

We formulate a similar isotopic mass conservation differential equation to simultaneously model changes in the sulfur and oxygen isotopic compositions of seawater sulfate at any given time:

$$\frac{d}{dt}\left(M_{SO_4}\cdot\delta^{34}S\right) = F_V\cdot\delta^{34}S_V + F_{WE}\cdot\delta^{34}S_{WE} + F_{WP}\cdot\delta^{34}S_{WP} - F_{BE}\cdot\delta^{34}S - F_{BP}\cdot\left(\delta^{34}S - \varepsilon_P\right), \quad (4)$$

where $\delta^{34}S$ denotes the sulfur isotopic composition of seawater sulfate; $\delta^{34}S_V$, $\delta^{34}S_{WE}$, *and* $\delta^{34}S_{WP}$ denote the sulfur isotopic compositions of volcanic degassing, evaporite weathering, and pyrite weathering, respectively; the sulfur isotopic composition of evaporite burial changes with seawater sulfate $\delta^{34}S$; ε_P denotes the global average S-isotope fractionation between seawater sulfate and pyrite.

$$\frac{d}{dt}\left(M_{SO_4}\cdot\delta^{18}O_{SO_4}\right) = F_V\cdot\delta^{18}O_V + F_{WE}\cdot\delta^{18}O_{WE} + F_{WP}\cdot\delta^{18}O_{WP} - F_{BE}\cdot\delta^{18}O_{SO_4} - F_{MSR}\cdot\delta^{18}O_{SO_4} + F_{REOX}\cdot\delta^{18}O_{REOX}, \quad (5)$$

where $\delta^{18}O_{SO_4}$ denotes the oxygen isotopic composition of seawater sulfate; $\delta^{18}O_V$, $\delta^{18}O_{WE}$, *and* $\delta^{18}O_{WP}$ denote the oxygen isotopic compositions of volcanic degassing, evaporite weathering, and pyrite weathering, respectively; the oxygen isotopic compositions of evaporite burial and the sulfate removed by MSR change with seawater sulfate $\delta^{18}O_{SO_4}$; $\delta^{18}O_{REOX}$ denotes the oxygen isotopic composition of sulfate reflux from sediments to the ocean.

To assess the effects of sea-level fluctuations on the global sulfur cycle, we take the fluxes (as well as isotopic values) that are affected by sea-level variations (i.e., pyrite weathering, pyrite burial, sulfate recycling) and divide them into two portions, one of which corresponds to the background flux while the other varies as a function of the extent of shelf area (A) (see Fig. 3 and SI). Despite highly variable amounts of pyrite in shelf sediments (0.1 to 1.8 wt%), we follow the assumption for ancient shales that the average pyrite sulfur concentration is 0.3 wt% (Berner, 1982). In proportion to shelf area lost during the EOT due to sea-level decline (Kominz et al., 2008), about 3×10^{21} g of shelf sediments has been eroded (Hay and Southam, 1977; Markovic et al., 2015). With a concentration of 0.3 wt% pyrite sulfur in the sediment, the initial shelf pyrite reservoir contains 3×10^{17} mol S (also see sensitivity test in SI). To set boundary (maximum and minimum) flux estimates, we assume that when shelf pyrite burial exceeds shelf pyrite weathering, this reservoir will be replenished continuously but not increase beyond 3×10^{17} mol S, whereas when increasing shelf pyrite weathering during sea-level low stands exceeds shelf pyrite burial and depletes the shelf pyrite reservoir, the total pyrite weathering flux is equal to the estimated continental pyrite weathering flux plus the flux from the shelf sub-reservoir until it is depleted. At the maximum extent of shelf area, 50% of sulfate recycling takes place in shelf sediments, and the other 50% takes place in slope and abyssal sediments (Fig. 3). The resulting maximum total reoxidation flux of 8.3×10^{13} mol/yr corresponding to the maximum shelf size is similar to the global estimate of 7.5×10^{13} mol/yr in modern sediments (Jørgensen and Kasten, 2006). We note that there are uncertainties in paleo-sea-level estimates due to regional and local subsidence or uplift, long-term ocean basin dynamics, and different hypsometry in the past. Supplementary materials contain analyses of how these uncertainties affect our results.

According to the inverse correlation between the global average S-isotope fractionation (ε_P) and shelf area (e.g., Leavitt et al., 2013, but see SI), we assume that all deep-sea sulfate reduction results in 50‰ fractionation and that all shelf sulfate reduction results in 35‰ fractionation (e.g., Kaplan et al., 1963; Leavitt et al., 2013). Thus, the global average pyrite $\delta^{34}S$ tends to increase when the shelf area expands, and vice versa.

Internal sulfate recycling modifies seawater sulfate $\delta^{18}O_{SO_4}$ microbially and/or abiotically. As indicated above, rather than specify the effect of each reaction, we treat the overall sulfate recycling as a black box and evaluate the cumulative effect on the O-isotope signature of sulfate reflux (i.e., $\delta^{18}O_{REOX}$), which corresponds to changes in shelf area. With an expansion of shelf area, the overall sulfate recycling is more dominated by microbially mediated processes, corresponding to a larger ^{18}O-enrichment in the sulfate reflux relative to seawater, and vice versa. In other words, sulfate reflux $\delta^{18}O_{REOX}$ is positively correlated to the extent of shelf area (see Fig. 3). We note that changes in the volume of ice sheets at the onset of the Antarctic cryosphere expansion exert additional influence on oceanic water $\delta^{18}O_{H_2O}$ (see SI).

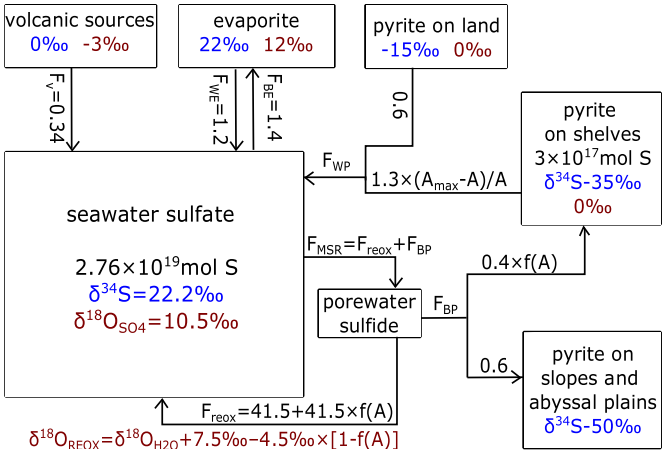

Fig. 3. A schematic of the box model for sulfur cycling, showing fluxes, isotopic compositions, and reservoir sizes. $f(A)=(A-A_{min})/(A_{max}-A_{min})$, where A_{max} and A_{min} represent the maximum and the minimum extent of shelf area between 37 and 31 Ma, respectively. Flux unit is 10^{12} mol/yr. S and O isotopic values are in blue and red, respectively. See details of the model description in SI and the steady-state numbers in Table 1. (For interpretation of the colors in the figure(s), the reader is referred to the web version of this article.)

We assume that the sulfur cycle is initially in a steady state with respect to the mass and isotopic ratios of seawater sulfate. The flux and isotopic ratio of all sulfate sources must equal the flux and isotopic ratio of all sulfate sinks:

$$F_{BP} = F_V + F_{WE} + F_{WP} - F_{BE}, \quad (6)$$

$$F_{BP}\cdot\left(\delta^{34}S-\varepsilon_P\right) = F_V\cdot\delta^{34}S_V + F_{WE}\cdot\delta^{34}S_{WE} + F_{WP}\cdot\delta^{34}S_{WP} - F_{BE}\cdot\delta^{34}S, \quad (7)$$

$$F_{REOX}\cdot\delta^{18}O_{REOX} = F_V\cdot\delta^{18}O_V + F_{WE}\cdot\delta^{18}O_{WE} + F_{WP}\cdot\delta^{18}O_{WP} - F_{BE}\cdot\delta^{18}O_{SO_4} - F_{MSR}\cdot\delta^{18}O_{SO_4}. \quad (8)$$

Using the fluxes and the associated isotopic values shown in Table 1, the model achieves mass and isotope equilibrium for a pyrite burial flux of 8.5×10^{11} mol/yr with a pyrite S-isotope value of −20.1‰. This corresponds to a global average seawater sulfate–pyrite fractionation of 42.3‰ (=22.2‰ + 20.1‰), which is well within the range between 30‰ and 60‰ used in previous sulfur cycle models (Kump and Garrels, 1986; Markovic et al., 2015; Rennie et al., 2018). With an estimated F_{REOX} of 6.7×10^{13} mol/yr, O-isotope equilibrium is achieved for a $\delta^{18}O_{REOX}$ value of 10.1‰.

4. Results

Our results show that between 38.5 and 34.5 Ma the S-isotope ratio of our marine barite samples is relatively stable, fluctuating around 22.3‰ (Fig. 4) with a standard deviation (1σ) of 0.2‰. Starting at 34.5 Ma the $\delta^{34}S$ value shows a steady decline of 0.6‰ from 22.3‰ to 21.7‰ at 33 Ma and remains stable at approximately 21.7‰ between 33 and 31.5 Ma. This is in line with the

Table 1
Modeled sulfate fluxes and isotope ratios for the initial steady state.

Parameter	Initial value	$\delta^{34}S$ [‰ VCDT]	$\delta^{18}O$ [‰ VSMOW]	Reference sources
V_{SO_4} = ocean volume	1.38×10^{21} L			[2]
$[SO_4]$ = seawater sulfate concentration	20 mM	22.2	10.5	[7, 14]
F_{WE} = evaporite weathering flux	1.2×10^{12} mol/yr	22	12	[4, 5, 13]
F_{WP} = pyrite weathering flux	7.6×10^{11} mol/yr[a]	−15	0	[5, 9]
F_V = volcanic degassing flux	3.4×10^{11} mol/yr	0	3	[6]
F_{BE} = evaporite burial flux	1.4×10^{12} mol/yr[a]	22.2	10.5	[4, 5, 13]
F_{BP} = pyrite burial flux	8.5×10^{11} mol/yr[a]	−20.1[a]		[3, 10]
F_{MSR} = sulfate influx for MSR in sediments	6.8×10^{13} mol/yr		10.5	[1, 8, 11, 12]
F_{REOX} = sulfate reflux out of sediments	6.7×10^{13} mol/yr[a]		10.1[a]	[8, 11, 12]

Note: V = volume, A = area, F = flux, $_W$ = weathering, $_B$ = burial, $_V$ = volcanic, $_E$ = evaporite, $_P$ = pyrite, $_{MSR}$ = microbial sulfate reduction, $_{REOX}$ = sulfide reoxidation.
[a] Values calculated as a function of shelf area. Reference sources: [1] Bowles et al., 2014; [2] Burke and Sengör, 1988; [3] Burke et al., 2018; [4] Claypool et al., 1980; [5] Garrel and Lerman, 1984; [6] Hansen and Wallman, 2003; [7] Horita et al., 2002; [8] Jørgensen and Kasten, 2006; [9] Kump and Garrels, 1986; [10] Leavitt et al., 2013; [11] Markovic et al., 2016; [12] Turchyn and Schrag, 2006; [13] Walker, 1986; [14] Wortmann and Paytan, 2012.

negative shift observed in the previous record (Paytan et al., 1998; and see SI).

Compared to $\delta^{34}S$, the $\delta^{18}O_{SO_4}$ value is more scattered, varying between 11.1‰ and 8.2‰ with an average value of 9.9‰ (Fig. 4). Between 38.5 and ~34.5 Ma, the $\delta^{18}O_{SO_4}$ value fluctuates around 10.2‰ with a standard deviation (1σ) of 0.5‰. We observe a clear negative excursion of 1.5‰ from 10.5‰ to ~9‰ between ~34.5 and 33 Ma, followed by a slight recovery to 9.5‰ at 31.5 Ma. The 95% confidence interval of the LOESS approximation for the "true" $\delta^{18}O_{SO_4}$ value is larger than that for $\delta^{34}S$, which is likely due to the variability of oxygen isotope data itself (Turchyn and Schrag, 2006; Markovic et al., 2016) and a smaller sample size for the $\delta^{18}O_{SO_4}$ record (average resolution of 120-kyr vs. 60-kyr). Although the data show considerable noise relative to the signal, statistical analysis with a student t-test demonstrates that the $\delta^{18}O_{SO_4}$ values before (38.5-34.5 Ma) and after (33-31.5 Ma) the EOT are statistically different (see SI). Moreover, the transient decrease of 1.5‰ is significantly larger than the analytical error (0.15‰).

5. Discussion

Our record shows a 0.6‰ decrease in $\delta^{34}S$ and a more pronounced 1.5‰ decrease in $\delta^{18}O_{SO_4}$ from the late Eocene to the early Oligocene. These negative shifts can be interpreted as the evidence for changes in biogeochemical sulfur cycling during the EOT, due to (i) a massive release of volcanic and/or hydrothermal sulfur to the ocean, (ii) an increase in oxidative weathering of sedimentary pyrite, and/or (iii) a reduction in pyrite burial on continental shelves.

Oxidation of volcanic sulfur volatiles (e.g., SO_2, H_2S) contributes sulfate with relatively low $\delta^{34}S$ and $\delta^{18}O_{SO_4}$ values to the ocean (Hansen and Wallman, 2003). Depending on the abundance and isotopic compositions of sulfur in eruptions, an increase in volcanic sulfur emission from 3.4×10^{11} to at least 1.2×10^{12} mol S/yr over 1.5 million years is required to account for the observed isotope shifts. The magnitude of the required change is, however, incompatible with the geological record, which is characterized by low spreading and subduction rates and relatively inactive intraplate volcanoes compared to other times during the Cenozoic (Larson, 1991; Hansen and Wallman, 2003).

Alternatively, land surface exposure due to mountain uplift and/or sea-level falls can increase pyrite weathering and thus change the flux of isotopically light sulfur into the ocean. Given the size of the marine sulfate reservoir and the comparatively small pyrite weathering flux, it is difficult to change the marine S-isotope ratio, unless there are basin-scale events like supercontinent breakup or the Indian-Eurasian collision (Wortmann et al., 2007; Wortmann and Paytan, 2012). However, we are not aware of any geological event during the EOT that would be capable of creating the necessary fluxes.

On the other hand, sea-level variations, which occur at a much faster rate than uplift, cause drastic changes in shelf area and constitute a major control of shelf pyrite weathering and pyrite burial on continental shelves (Turchyn and Schrag, 2006; Markovic et al., 2015; Kölling et al., 2019). Following the initiation of the long-term Cenozoic cooling trend, the increase in Antarctic ice volume is accompanied by a global sea-level retreat. Estimates for the maximum sea-level drop at the EOT range between 50 and 100 m, with an equivalent average drop of 40 ± 10 m from the late-Eocene to early-Oligocene (e.g., Zachos et al., 2001; Kominz et al., 2008; Miller et al., 2020). In response to the sea-level decline, the global shelf area is reduced by up to 40% (Fig. 5). This magnitude of shelf-area reduction is about two-thirds of that during Pleistocene glaciations, where global sea-level drops by up to 130-150 m below the present-day sea level (equivalent average drop = 60 m) result in up to 60% reduction of the global shelf area (Table 2; Markovic et al., 2015; Miller et al., 2020). Falling sea levels result in a transfer of shelf sediments to the continental slope and/or abyssal plain. Hay and Southam (1977) estimate that during the Pleistocene up to 5×10^{21} g of sediments has been removed from the shelves. While similar estimates of shelf sediment erosion for the EOT are not available, as a first-order approximation, the above values suggest that sediment loss is on the order of 50 to 70% of that in the Pleistocene.

It is noteworthy that due to the long residence time of sulfate in the ocean, the seawater $\delta^{34}S$ signal reflects the average sea-level response integrated over several million years. In other words, regardless of the maximum sea-level drop reported across the EOT (e.g., 90 m in Kominz et al., 2008), the equivalent average sea-level change of 40 ± 10 m between the late Eocene and the early Oligocene primarily controls the magnitude of the $\delta^{34}S$ excursion (see SI for details). This is the same for the seawater sulfate $\delta^{18}O_{SO_4}$ signal but to a lesser degree. In the following, we thus cast our discussion in terms of the average changes from the late Eocene to early Oligocene (but also see maximum changes in Table S1).

5.1. Effects of sea-level changes on sulfur cycling

Subaerial exposure and erosion of the previously submerged shelf sediment facilitate oxidative weathering of pyrite (Markovic et al., 2015; Torres et al., 2017). Following the assumption of 0.3 wt% pyrite sulfur in shelf sediments (after Markovic et al., 2015), quantitative modeling suggests that the sea-level drop has caused

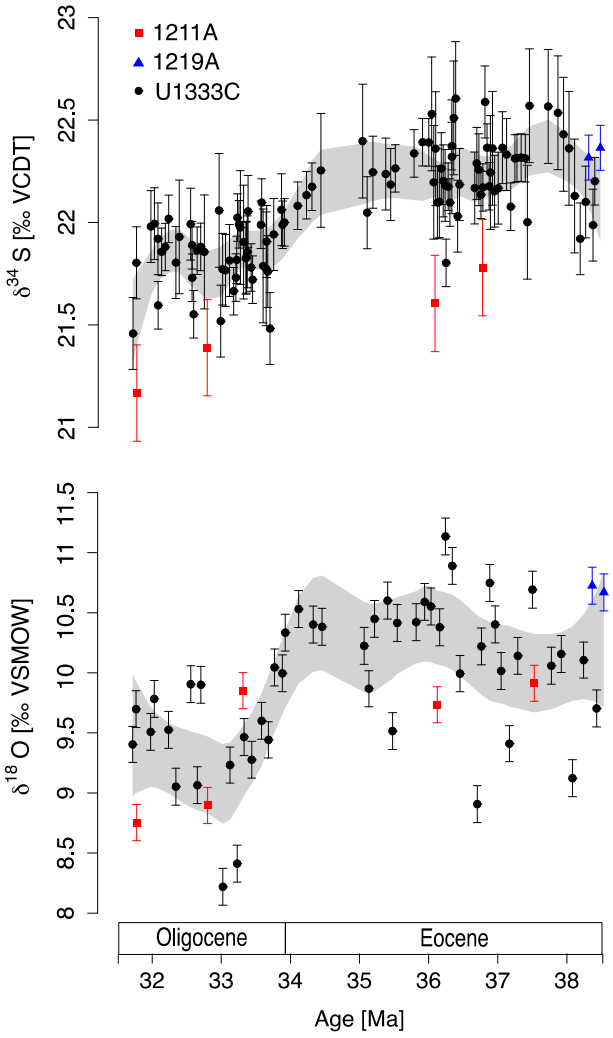

Fig. 4. S and O isotope data from marine barite between 38.5 and 31.5 Ma. Red squares denote ODP Hole 1211A; blue triangles denote ODP Hole 1219A; black circles denote IODP Hole U1333C. The gray envelopes represent the 95% confidence interval of the LOESS regression with the optimal "span" value of 0.3 for δ^{34}S and 0.45 for $\delta^{18}O_{SO_4}$. All the data are mapped on the GTS2012 timescale (Gradstein et al., 2012). The small offset in δ^{34}S between 1211A and U1333C is likely due to natural variabilities and/or analytical errors (see SEM images and student t-tests in SI). We report data with error bars (1σ) produced by repeated measurements of the standards in the same run; the consistent temporal trend supports the secular nature of the record despite the small range of the values compared to the errors. The δ^{34}S plot includes 15 data points published in Yao et al. (2020) in addition to this study (see Table S2).

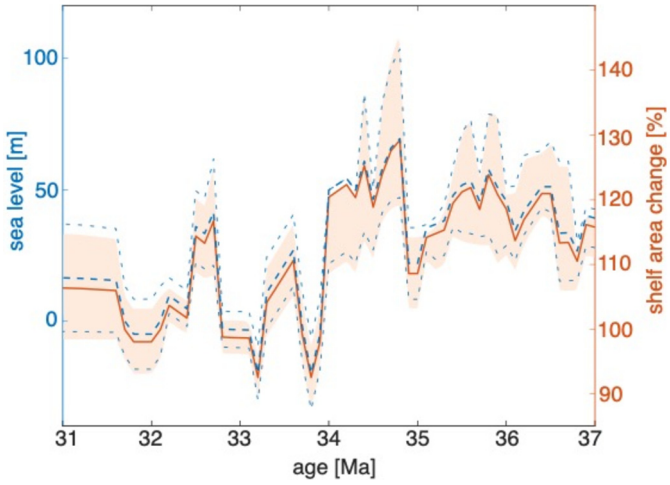

Fig. 5. Sea-level variations and the corresponding changes in shelf area between 37 and 31 Ma. Shelf size at any given time step is calculated as a function of the estimated sea level. Blue dashed lines are the backstripped sea levels with best-imaginary lowstands and the upper and lower error bounds after Kominz et al. (2008); orange line with shaded area is the shelf size corresponding to the best-estimate sea level, enveloped by the uncertainties calculated from the minimum and maximum sea-level estimates. Age uncertainties are of ±0.5 million years (Kominz et al., 2008). See SI for details.

reoxidation of 2.5 × 10^{17} mol sulfur from pyrite back to sulfate by 33 Ma (Fig. 6c; also see SI), contributing to ~0.5‰ decline in the observed S-isotope signal (Fig. 6f) and rising the seawater sulfate concentration from about 19.8 to 20.2 mM (Fig. 6e). With an increase in pyrite weathering flux by ~22% (i.e., from an average of 7 × 10^{11} mol/yr at the late-Eocene sea-level highstands to an average of 9 × 10^{11} mol/yr at the early-Oligocene sea-level lowstands, see Fig. 6a), more isotopically depleted sulfur is transferred to the ocean. Concurrently with intensified pyrite weathering on freshly exposed shelves, pyrite burial during sea-level low stands is confined to the remnant submerged shelf and deeper regions of the ocean (e.g., slopes and abyssal plains), which are generally considered to be unfavorable to pyrite burial (Canfield et al., 1992; Jørgensen, 1982). Consequently, the global average pyrite burial decreases. In our model, we assume that the pyrite burial rate in and below the minimum submerged regions is constant at 6 × 10^{11} mol/yr, and that the pyrite burial rate in the shallower shelf regions varies as a function of shelf area to up to 4 × 10^{11} mol/yr. With these assumptions, the EOT sea-level drop would be equivalent to an average 19% reduction of the global pyrite burial rate (Fig. 6b). While changes in shelf area may also affect S-isotope fractionation between seawater sulfate and pyrite by ~7‰ (Fig. 6d), model results suggest that the primary driver of the δ^{34}S decline is the mass transfer from sedimentary pyrite to seawater sulfate but not changes in isotopic fractionation (see SI).

Changes in shelf area also affect O-isotope ratios of seawater sulfate. This is because i) Oxidative pyrite weathering creates sulfate with a $\delta^{18}O_{SO_4}$ value close to the ambient water where the oxidation occurs. Based on our model, this process accounts for 20-25% of the observed $\delta^{18}O_{SO_4}$ signal (see SI for details.) ii) The areal extent of continental shelves controls sulfate oxygen turnover through MSR and sulfide reoxidation, fluxes of which are one to two orders of magnitude larger than the pyrite fluxes (i.e., 4 × 10^{13} to 8 × 10^{13} mol/yr; see Fig. 7a and e). This will reduce the residence time of sulfate bound oxygen in the ocean to 0.3-0.7 million years, which is in broad agreement with our observation that the $\delta^{18}O_{SO_4}$ signal responds rapidly to changes in shelf area (Fig. 7f).

By further taking the effects of cumulative ^{18}O-enrichment during sulfate recycling and oceanic water $\delta^{18}O_{H_2O}$ variations (see SI) into account, our model captures the shape and magnitude of the $\delta^{18}O_{SO_4}$ excursion (Fig. 7f). The recycled sulfate $\delta^{18}O_{SO_4}$ varies from ~10.5‰ before 34 Ma to ~9‰ at lower sea levels after 34 Ma (Fig. 7b). These values agree well with the previous estimate (7-17‰; Turchyn and Schrag, 2006) and are in line with the range of sulfate $\delta^{18}O_{SO_4}$ in marine sediment porewater (e.g., Antler et al., 2013). In other words, the ~1.5‰ decrease in recycled sulfate $\delta^{18}O_{SO_4}$ requires a more significant contribution of abiotic sulfide reoxidation to the overall sulfate recycling (Fig. 7c, from 15% to ~30%) at the expense of microbially mediated processes (Fig. 7d, from 85% to ~70%), underpinning a shift towards more oxygenated organic matter deficient deep-sea seafloor environments. This shift supports the reduction in pyrite formation as indicated above based on the δ^{34}S data and is also consistent with the decline in shelf-hosted sedimentary denitrification due to a loss of submerged continental shelves at the EOT as depicted from marine N-isotope rations (Kast et al., 2019).

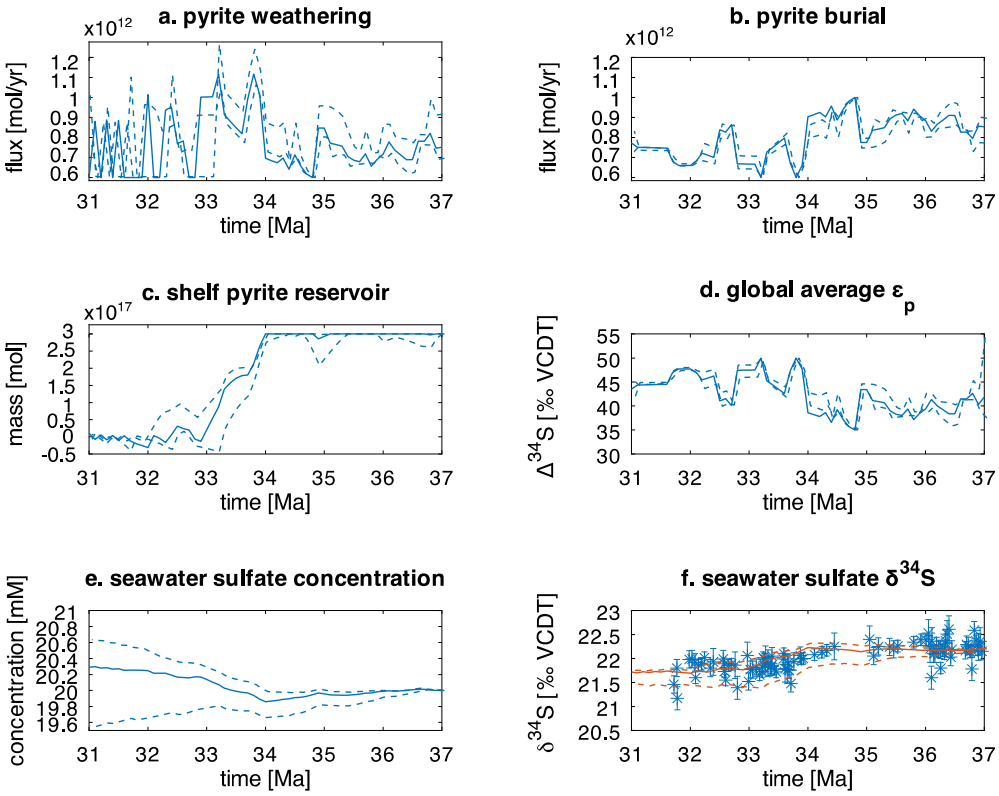

Fig. 6. Model results depicting the transfer of sulfur from sedimentary pyrite to dissolved seawater sulfate between 37 and 31 Ma. (a) Pyrite weathering; (b) Pyrite burial; (c) Pyrite reservoir on continental shelves; (d) Global average S-isotope fractionation between seawater sulfate and pyrite; (e) Seawater sulfate concentration; (f) Modeled seawater sulfate $\delta^{34}S$ values versus our measurements (asterisk symbols). Dashed lines show the error envelopes for model outputs resulted from uncertainties in sea-level reconstruction.

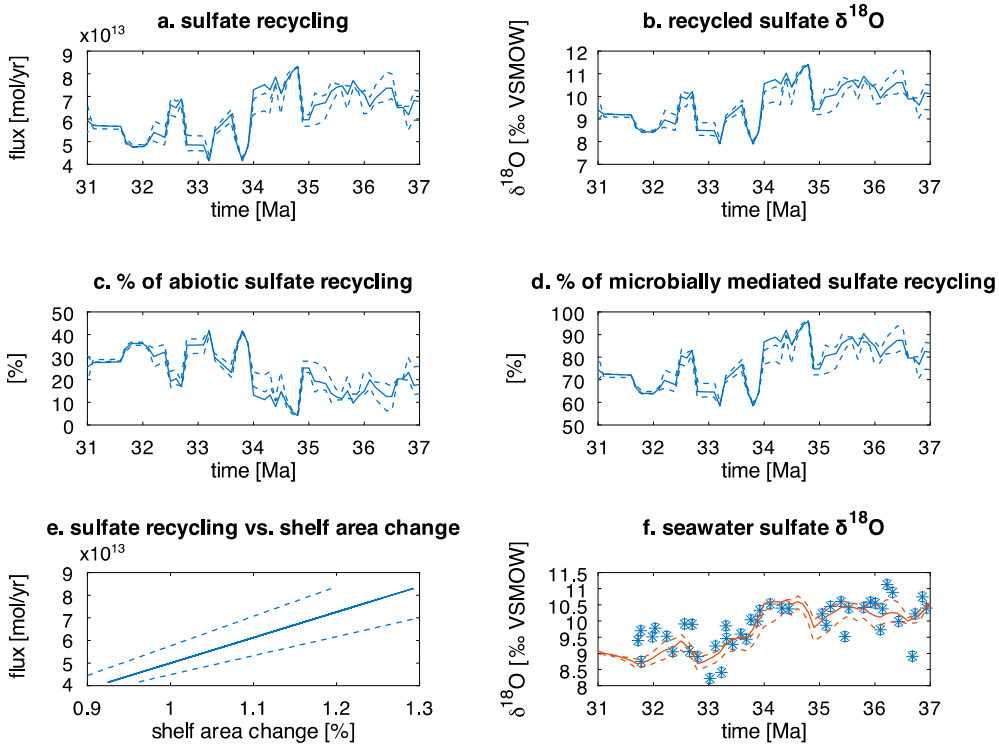

Fig. 7. Model results depicting internal sulfate recycling impacts on $\delta^{18}O_{SO_4}$ between 37 and 31 Ma. (a) Sulfate reflux from sediments to the ocean; (b) Sulfate reflux $\delta^{18}O_{REOX}$; (c) The portion of abiotic sulfate recycling to overall sulfate recycling; (d) The portion of microbially mediated sulfate recycling to overall sulfate recycling; (e) Correlation between sulfate reflux and shelf area; (f) Modeled seawater sulfate $\delta^{18}O_{SO_4}$ values versus our measurements (asterisk symbols). Dashed lines show the error envelopes for model outputs resulted from uncertainties in sea-level reconstruction.

5.2. Shelf pyrite oxidation and the release of CO_2 during sea-level low stands

Pyrite oxidation in shelf sediments proceeds through reactions similar to those at acid mine drainage. Specifically, pyrite weathering produces sulfuric acid, which is subsequently neutralized by carbonate dissolution (Berner, 1982; Garrel and Lerman, 1984). It has been suggested that this process might be a source of CO_2 over geological timescales (Torres et al., 2014; Markovic et al., 2015) or even instrumental in triggering glacial terminations (Kölling et al., 2019).

Initially, the reaction converts pyrite into sulfuric acid ($4FeS_2 + 15O_2 + 14H_2O \rightarrow 4Fe(OH)_3 + 8H_2SO_4$); subsequently, however, reactions may proceed in several ways:

- In the presence of carbonate minerals, the sulfuric acid can react to carbonates through $H_2SO_4 + CaCO_3 \rightarrow SO_4^{2-} + Ca^{2+} + CO_2 + H_2O$. This reaction produces 2 mol CO_2 per mol pyrite and will increase marine dissolved inorganic carbon (DIC) and pCO_2 accordingly.
- Alternatively, if the sulfuric acid reacts to carbonates through $H_2SO_4 + 2CaCO_3 \rightarrow SO_4^{2-} + 2Ca^{2+} + 2HCO_3^-$, it will produce 4 mol HCO_3^- per mol pyrite, but the effect on pCO_2 is compensated by the concomitant increase of 4 mol alkalinity.
- In the absence of carbonate minerals buffering pH, pyrite oxidation can proceed through ferric iron ($FeS_2 + 14Fe^{3+} + 8H_2O \rightarrow 15Fe^{2+} + 2SO_4^{2-} + 16H^+$). In this scenario, the release of surplus protons is not compensated by increased alkalinity, which will also increase pCO_2.

Torres et al. (2017) analyzed the globally averaged weathering data for the LGM and concluded that the net contribution of pyrite oxidation-derived CO_2 during glacial lowstands might have been on the order of 25 ppm to 80 ppm CO_2 over 10 kyrs. The pyrite oxidation fluxes considered by Torres et al. (2017) are on the order of 2.5×10^{11} to 7.5×10^{11} mol S/yr, whereas we estimate 6×10^{11} to 1.2×10^{12} mol S/yr.

It is, however, difficult to relate pyrite oxidation fluxes to changes in pCO_2 directly. This is not only a question of the actual reaction pathways, but also how fast we introduce any unbuffered DIC. The Kominz et al. (2008) data, for example, appears to suggest a major (and sustained) sea-level drop at the Oligocene boundary. In this case, much of the pyrite oxidation would happen within a few thousand years, and the impact on the marine carbon system would be substantial. On the other hand, if pyrite oxidation happened over several million years, the increased CO_2 flux would be compensated in the ocean by small changes in the carbonate compensation depth (CCD).

While there is considerable uncertainty with respect to the timing and magnitude of the global sea-level variations, our $\delta^{18}O_{SO_4}$ shows the best fit if we assume a major sea-level adjustment across the Eocene/Oligocene boundary (see Fig. 7). Likewise, there is uncertainty about the exact reaction stoichiometry, and an in-depth analysis of the marine carbonate system is beyond the scope of this paper. However, we do point out that the sulfide oxidation fluxes obtained from our model are of a similar magnitude to those considered for the glacial/interglacial changes of the Pleistocene (see Table 2; e.g., Markovic et al., 2015; Kölling et al., 2019) and likely affect the carbonate chemistry of the Eocene/Oligocene ocean.

6. Conclusion

This study shows that the emergent icehouse conditions during the Eocene-Oligocene transition are accompanied by a −0.6‰ shift in seawater sulfate $\delta^{34}S$ and a −1.5‰ shift in seawater sulfate $\delta^{18}O_{SO_4}$. We argue that ice growth and the concomitant sea-level drop reduce shelf areas by up to 40%. This reduces the total sulfur burial flux, and most importantly, reoxidized previously buried sulfides. While the loss of submerged continental shelves may increase the globally averaged S-isotope offset between seawater and pyrite, its effect on seawater $\delta^{34}S$ is more than compensated by the oxidation of pyrite in subaerially exposed shelf sediments, which transfers isotopically light S from the sedimentary pyrite reservoir back into the marine dissolved sulfate reservoir. Box modeling shows that the shelf area contraction across the EOT and the net transfer of sulfur (2.5×10^{17} mol) from the shelf to the open ocean are responsible for the observed seawater sulfate $\delta^{34}S$ shift from 22.3‰ to 21.7‰ (VCDT) and the concomitant decrease in seawater sulfate $\delta^{18}O_{SO_4}$ from 10.5‰ to 8.7‰ (VSMOW). Furthermore, oxidation of sedimentary pyrite results in the formation of up to 24,500 Gt sulfuric acid, which will have a substantial effect on the marine carbonate system. While it is beyond the scope of our study to evaluate how this would have quantitatively affected atmospheric pCO_2, we note that CO_2 generation during pyrite oxidation may constitute a stabilizing feedback mechanism during ice-sheet expansion.

Table 2
Comparison between the oxidation of sedimentary pyrite on continental shelves during the EOT and Pleistocene glaciations. Depending on the reaction pathways of pyrite oxidation and carbonate dissolution, oxidation of 8,000 Gt sulfur from shelf sedimentary pyrite on continental shelves to sulfate can dissolve 25,000 to 100,000 Gt $CaCO_3$.

Changes	EOT		Pleistocene	
	max.	avg.	max.	avg.
Sea level [m]	−90	−40	−120	−60
Shelf area	−40%	−16%	−60%	−28%
Pyrite weathering flux	+83%	+22%	+120%	+33%
Pyrite burial flux	−40%	−19%	−65%	−34%
Shelf pyrite reservoir [Gt S]	−8,000		−19,200 (−13,120)[a]	
Sulfuric acid release [Gt H_2SO_4]	+24,500		+58,800 (+40,180)[a]	

Note: Numbers for the Pleistocene S model are after Markovic et al., 2015.
[a] The estimates after Kölling et al. (2019).

CRediT authorship contribution statement

Weiqi Yao: Conceptualization, Data curation, Methodology, Software, Visualization, Writing – original draft. **Stefan Markovic:** Data curation, Methodology, Software, Writing – original draft. **Adina Paytan:** Funding acquisition, Resources, Writing – review & editing. **Andrea M. Erhardt:** Methodology, Writing – review & editing. **Ulrich G. Wortmann:** Conceptualization, Validation, Writing – review & editing.

Declaration of competing interest

The authors declare that they have no known competing financial interests or personal relationships that could have appeared to influence the work reported in this paper.

Acknowledgements

We thank H. Li for her support with isotope analyses. This work was supported by a Discovery Grant of the Natural Sciences and Engineering Research Council of Canada (NSERC) grant RGPIN-2018-05873 to U.G.W. and the National Science Foundation (NSF) CAREER grant OCE-0449732 to A.P.

Appendix A. Supplementary material

Supplementary material related to this article can be found online at https://doi.org/10.1016/j.epsl.2021.117015.

References

Antler, G., Turchyn, A.V., Rennie, V.C.F., Herut, B., Sivan, O., 2013. Coupled sulfur and oxygen isotope insight into bacterial sulfate reduction in the natural environment. Geochim. Cosmochim. Acta 118, 98–117. https://doi.org/10.1016/j.gca.2013.05.005.

Balci, N., Mayer, B., Shanks, W.C., Mandernack, K.W., 2012. Oxygen and sulfur isotope systematics of sulfate produced during abiotic and bacterial oxidation of sphalerite and elemental sulfur. Geochim. Cosmochim. Acta 77, 335–351. https://doi.org/10.1016/j.gca.2011.10.022.

Basak, C., Martin, E.E., 2013. Antarctic weathering and carbonate compensation at the Eocene–Oligocene transition. Nat. Geosci. 6, 121–124. https://doi.org/10.1038/NGEO1707.

Berner, R.A., 1982. Burial of organic-carbon and pyrite sulfur in the modern ocean - its geochemical and environmental significance. Am. J. Sci. 282, 451–473. https://doi.org/10.2475/ajs.282.4.451.

Böttcher, M.E., Brumsack, H.-J., de Lange, G.J., 1998. Sulfate reduction and related stable isotope (^{34}S, ^{18}O) variations in interstitial waters from the eastern Mediterranean. In: Robertson, A.H.F., et al. (Eds.), Proceedings of the Ocean Drilling Program, Scientific Results, vol. 160. Texas A & M University, Ocean Drilling Program, College Station, Texas, pp. 365–373.

Böttcher, M.E., Thamdrup, B., 2001. Anaerobic sulfide oxidation and stable isotope fractionation associated with bacterial sulfur disproportionation in the presence of MnO_2. Geochim. Cosmochim. Acta 65, 1573–1581. https://doi.org/10.1016/S0016-7037(00)00622-0.

Böttcher, M.E., Thamdrup, B., Gehre, M., Theune, A., 2005. $^{34}S/^{32}S$ and $^{18}O/^{16}O$ fractionation during sulfur disproportionation by Desulfobulbus propionicus. Geochem. J. 22, 219–226. https://doi.org/10.1080/01490450590947751.

Bowles, M.W., Mogollón, J.M., Kasten, S., Zabel, M., Hinrichs, K.-U., 2014. Global rates of marine sulfate reduction and implications for sub–sea-floor metabolic activities. Science 344, 889–891. https://doi.org/10.1126/science.1249213.

Bralower, T.J., Premoli Silva, I., Malone, M.J., et al., 2002. Site 1211. In: Proceedings of the Ocean Drilling Program, Initial Reports, vol. 198. Texas A & M University, Ocean Drilling Program, College Station, Texas, pp. 1–81.

Brand, W.A., Coplen, T.B., Vogl, J., Rosner, M., Prohaska, T., 2014. Assessment of international reference materials for isotope-ratio analysis (IUPAC Technical Report). Pure Appl. Chem. 86, 425–467. https://doi.org/10.1515/pac-2013-1023.

Brunner, B., Bernasconi, S.M., Kleikemper, J., Schroth, M., 2005. A model for oxygen and sulfur isotope fractionation in sulfate during bacterial sulfate reduction processes. Geochim. Cosmochim. Acta 69, 4773–4785. https://doi.org/10.1016/j.gca.2005.04.017.

Burke, K., Sengör, A.M.C., 1988. Ten metre global sea-level change associated with South Atlantic Aptian salt deposition. Mar. Geol. 83, 309–312. https://doi.org/10.1016/0025-3227(88)90064-3.

Burke, A., Present, T.M., Paris, G., Rae, E.C.M., Sandilands, B.H., Gaillardet, J., Peucker-Ehrenbrink, B., Fischer, W.W., McClelland, J.W., Spencer, R.G.M., Voss, B.M., Adkins, J.F., 2018. Sulfur isotopes in rivers: insights into global weathering budgets, pyrite oxidation, and the modern sulfur cycle. Earth Planet. Sci. Lett. 496, 168–177. https://doi.org/10.1016/j.epsl.2018.05.022.

Canfield, D.E., Raiswell, R., Bottrell, S., 1992. The reactivity of sedimentary iron minerals toward sulfide. Am. J. Sci. 292, 659–683. https://doi.org/10.2475/ajs.292.9.659.

Chambers, L.A., Trudinger, P.A., 1979. Microbiological fractionation of stable sulfur isotopes: a review and critique. Geomicrobiol. J. 1, 249–293. https://doi.org/10.1080/01490457909377735.

Claypool, G.E., Holser, W.T., Kaplan, I.R., Sakai, H., Zak, I., 1980. The age curves of sulfur and oxygen isotopes in marine sulfate and their mutual interpretation. Chem. Geol. 28, 199–260. https://doi.org/10.1016/0009-2541(80)90047-9.

Cleveland, W.S., 1979. Robust locally weighted regression and smoothing scatter plots. J. Am. Stat. Assoc. 74, 829–836.

Coxall, H.K., Pearson, P.N., 2007. The Eocene-Oligocene transition. In: Williams, M., et al. (Eds.), Deep Time Perspectives on Climate Change: Marrying the Signal From Computer Models and Biological Proxies. Geol. Soc., London, pp. 351–387.

DeConto, R.M., Pollard, D., 2003. Rapid Cenozoic glaciation of Antarctica induced by declining atmospheric CO_2. Nature 421, 245–249. https://doi.org/10.1038/nature01290.

Fritz, P., Basharmal, G.M., Drimmie, R.J., Ibsen, J., Qureshi, R.M., 1989. Oxygen isotope exchange between sulphate and water during bacterial reduction of sulphate. Chem. Geol. 79, 99–105. https://doi.org/10.1016/0168-9622(89)90012-2.

Garrel, R.M., Lerman, A., 1984. Coupling of the sedimentary sulfur and carbon cycles - an improved model. Am. J. Sci. 284, 989–1007. https://doi.org/10.2475/ajs.284.9.989.

Goldhaber, M.B., Kaplan, I.R., 1975. Controls and consequences of sulfate reduction rates in recent marine sediments. Soil Sci. 119, 42–55. https://doi.org/10.2136/sssaspecpub10.c2.

Gradstein, F.M., Ogg, J.G., Schmitz, M., Ogg, G., 2012. The Geologic Time Scale 2012. Elsevier Academic Press, Amsterdam, p. 1176.

Hansen, K.W., Wallman, K., 2003. Cretaceous and Cenozoic evolution of seawater composition, atmospheric O_2 and CO_2 - a model perspective. Am. J. Sci. 303, 94–148. https://doi.org/10.2475/ajs.303.2.94.

Hay, W.W., Southam, J.R., 1977. Modulation of marine sedimentation by the continental shelves. In: Andersen, N.R., Malahoff, A. (Eds.), The Fate of Fossil Fuel CO_2 in the Oceans. Plenum Press, New York, pp. 569–604.

Hay, W.W., Migdisov, A., Balukhovsky, A.N., Wold, C.N., Flögel, S., Söding, E., 2006. Evaporites and the salinity of the ocean during the Phanerozoic: implications for climate, ocean circulation and life. Palaeogeogr. Palaeoclimatol. Palaeoecol. 240, 3–46. https://doi.org/10.1016/j.palaeo.2006.03.044.

Horita, J., Zimmermann, H., Holland, H.D., 2002. Chemical evolution of seawater during the Phanerozoic: implications from the record of marine evaporites. Geochim. Cosmochim. Acta 66, 3733–3756. https://doi.org/10.1016/S0016-7037(01)00884-5.

Ivany, L.C., Van Simaeys, S., Domack, E.W., Samson, S.D., 2006. Evidence for an earliest Oligocene ice sheet on the Antarctic Peninsula. Geology 34, 377–380. https://doi.org/10.1130/G22383.1.

Jørgensen, B.B., 1982. Mineralization of organic-matter in the sea bed - the role of sulfate reduction. Nature 296, 643–645. https://doi.org/10.1130/G22383.1.

Jørgensen, B.B., Kasten, S., 2006. Sulfur cycling and methane oxidation. In: Schulz, H.D., Zabel, M. (Eds.), Marine Geochemistry, 2nd Edition. Springer, Berlin, Germany, pp. 271–309.

Kaplan, I.R., Emery, K.O., Rittenberg, S.C., 1963. The distribution and isotopic abundance of sulphur in recent marine sediments off southern California. Geochim. Cosmochim. Acta 27, 297–331. https://doi.org/10.1016/0016-7037(63)90074-7.

Kaplan, I.R., Rittenberg, S.C., 1964. Microbiological fractionation of sulphur isotopes. J. Gen. Microbiol. 34, 195–212. https://doi.org/10.1099/00221287-34-2-195.

Katz, M.E., Miller, K.G., Wright, J.D., Wade, B.S., Browning, J.V., Cramer, B.S., Rosenthal, Y., 2008. Stepwise transition from the Eocene greenhouse to the Oligocene icehouse. Nat. Geosci. 1, 330–334. https://doi.org/10.1038/ngeo179.

Kast, E.R., Stolper, D.A., Auderset, A., Higgins, J.A., Ren, H., Wang, X.T., Martínez-García, A., Haug, G.H., Sigman, D.M., 2019. Nitrogen isotope evidence for expanded Ocean Suboxia in the Early Cenozoic. Science 364, 386–389. https://doi.org/10.1126/science.aau5784.

Kennett, J.P., Shackleton, N.J., 1976. Oxygen isotopic evidence for the development of the psychrosphere 38 Myr ago. Nature 260, 513–515. https://doi.org/10.1038/260513a0.

Kölling, M., Bouimetarhan, I., Bowles, M.W., et al., 2019. Consistent CO_2 release by pyrite oxidation on continental shelves prior to glacial terminations. Nat. Geosci. 12, 929–934. https://doi.org/10.1038/s41561-019-0465-9.

Kominz, M.A., Browning, J.V., Miller, K.G., Sugarman, P.J., Mizintseva, S., Scotese, C.R., 2008. Late Cretaceous to Miocene sea-level estimates from the New Jersey and Delaware coastal plain coreholes: an error analysis. Basin Res. 20, 211–226. https://doi.org/10.1111/j.1365-2117.2008.00354.x.

Kump, L.R., Garrels, R.M., 1986. Modeling atmospheric O_2 in the global sedimentary redox cycle. Am. J. Sci. 286, 337–360. https://doi.org/10.2475/ajs.286.5.337.

Larson, R.L., 1991. Geological consequences of superplumes. Geology 19, 963–966. https://doi.org/10.1130/0091-7613(1991)019<0963:GCOS>2.3.CO;2.

Leavitt, W.D., Halevy, I., Bradley, A.S., Johnston, D.T., 2013. Influence of sulfate reduction rates on the Phanerozoic sulfur isotope record. Proc. Natl. Acad. Sci. USA 110, 11244–11249. https://doi.org/10.1073/pnas.1218874110.

Liu, Z., Pagani, M., Zinniker, D., DeConto, R., Huber, M., Brinkhuis, H., Shah, S.R., Leckie, R.M., Pearson, A., 2009. Global cooling during the Eocene-Oligocene climate transition. Science 323, 1187–1190. https://doi.org/10.1126/science.1166368.

Lloyd, R.M., 1968. Oxygen isotope behaviour in the sulfate-water system. J. Geophys. Res. 73, 6099–7110. https://doi.org/10.1029/JB073i018p06099.

Lyle, M., Wilson, P.A., Janecek, T.R., et al., 2002. Site 1219. In: Proceedings of the Ocean Drilling Program, Initial Reports, vol. 199. Texas A & M University, Ocean Drilling Program, College Station, Texas, pp. 1–129.

Markovic, S., Paytan, A., Li, H., Wortmann, U.G., 2016. A revised seawater sulfate oxygen isotope record for the last 4 Myr. Geochim. Cosmochim. Acta 175, 239–251. https://doi.org/10.1016/j.gca.2015.12.005.

Markovic, S., Paytan, A., Wortmann, U.G., 2015. Pleistocene sediment of floading and the global sulfur cycle. Biogeosciences 12, 3043–3060. https://doi.org/10.5194/bg-12-3043-2015.

Miller, K.G., Browning, J.V., Schmelz, W.J., Kopp, R.E., Mountain, G.S., Wright, J.D., 2020. Cenozoic sea-level and cryospheric evolution from deep-sea geochemical and continental margin records. Sci. Adv. 6, eaaz1346. https://doi.org/10.1126/sciadv.aaz1346.

Miller, K.G., Fairbanks, R.G., Mountain, G.S., 1987. Tertiary oxygen isotope synthesis, sea level history, and continental margin erosion. Paleoceanography 2, 1–19. https://doi.org/10.1029/PA002i001p00001.

Mizutani, Y., Rafter, T.A., 1973. Isotopic behaviour of sulphate oxygen in the bacterial reduction of sulphate. Geochem. J. 6, 183–191. https://doi.org/10.2343/geochemj.6.183.

Pälike, H., Lyle, M., Nishi, H., et al., 2010. Site U1333. In: Proceedings of the Integrated Ocean Drilling Program, Initial Reports, vol. 320/321. Texas A & M University, Ocean Drilling Program, College Station, Texas, pp. 1–93.

Paytan, A., Kastner, M., Campbell, D., Thiemens, M.H., 1998. Sulfur isotopic composition of Cenozoic seawater sulfate. Science 282, 1459–1462. https://doi.org/10.1126/science.282.5393.1459.

Paytan, A., Kastner, M., Martin, E.E., Macdougall, J.D., Herbert, T., 1993. Marine barite as a monitor of seawater strontium isotope composition. Nature 366, 445–449. https://doi.org/10.1038/366445a0.

Rennie, V.C.F., Paris, G., Sessions, A.L., Abramovich, A., Turchyn, A.V., Adkins, J.F., 2018. Cenozoic record of $\delta^{34}S$ in foraminiferal calcite implies an early Eocene shift to deep-ocean sulfide burial. Nat. Geosci. 11, 761–765. https://doi.org/10.1038/s41561-018-0200-y.

Sim, M.S., Bosak, T., Ono, S., 2011. Large sulfur isotope fractionation does not require disproportionation. Science 333, 74–77. https://doi.org/10.1126/science.1205103.

Torres, M.A., Moosdorf, N., Hartmann, J., Adkins, J.F., West, A.J., 2017. Glacial weathering, sulfide oxidation, and global carbon cycle feedbacks. Proc. Natl. Acad. Sci. USA 114, 8716–8721. https://doi.org/10.1073/pnas.1702953114.

Torres, M.A., West, A.J., Li, G., 2014. Sulphide oxidation and carbonate dissolution as a source of CO_2 over geological timescales. Nature 507, 346–349. https://doi.org/10.1038/nature13030.

Turchyn, A.V., Schrag, D.P., 2006. Cenozoic evolution of the sulfur cycle: insight from oxygen isotopes in marine sulfate. Earth Planet. Sci. Lett. 241, 763–779. https://doi.org/10.1016/j.epsl.2005.11.007.

Van Stempvoort, D.R., Krouse, H.R., 1994. Controls of $\delta^{18}O$ in sulfate - review of experimental data and application to specific environments. In: Alpers, C.N., Blowes, D.W. (Eds.), Environmental Geochemistry of Sulfide Oxidation, vol. 550. American Chemical Society, Washington, D.C., pp. 446–480.

Walker, J.C.G., 1986. Global geochemical cycles of carbon, sulfur, and oxygen. Mar. Geol. 70, 159–174. https://doi.org/10.1016/0025-3227(86)90093-9.

Wankel, S.D., Bradley, A.S., Eldridge, D.L., Johnston, D.T., 2014. Determination and application of the equilibrium oxygen isotope effect between water and sulfite. Geochim. Cosmochim. Acta 125, 694–711. https://doi.org/10.1016/j.gca.2013.08.039.

Wortmann, U.G., Chernyavsky, B.M., Bernasconi, S.M., Brunner, B., Böttcher, M.E., Swart, P.K., 2007. Oxygen isotope biogeochemistry of pore water sulfate in the deep biosphere: dominance of isotope exchange reactions with ambient water during microbial sulfate reduction (ODP Site 1130). Geochim. Cosmochim. Acta 71, 4221–4232. https://doi.org/10.1016/j.gca.2007.06.033.

Wortmann, U.G., Paytan, A., 2012. Rapid variability of seawater chemistry over the past 130 million years. Science 337, 334–336. https://doi.org/10.1126/science.1220656.

Yao, W., Paytan, A., Griffith, E.M., Martínez-Ruiz, F., Markovic, S., Wortmann, U.G., 2020. A revised seawater sulfate S-isotope curve for the Eocene. Chem. Geol. 532, 119382. https://doi.org/10.1016/j.chemgeo.2019.119382.

Zachos, J.C., Pagani, M., Sloan, L., Thomas, E., Billups, K., 2001. Trends, rhythms, and aberrations in global climate 65 Ma to present. Science 292, 686–693. https://doi.org/10.1126/science.1059412.

Zeebe, R.E., 2010. A new value for the stable oxygen isotope fractionation between dissolved sulfate ion and water. Geochim. Cosmochim. Acta 74, 818–828. https://doi.org/10.1016/j.gca.2009.10.034.